Microchim Acta (2012) 178:277–283
DOI 10.1007/s00604-012-0834-1

ORIGINAL PAPER

Electrochemistry and biosensing activity of cytochrome c immobilized on a mesoporous interface assembled from carbon nanospheres

Ying Wang · Xiaojun Bian · Lei Liao · Jie Zhu · Kai Guo · Jilie Kong · Baohong Liu

Received: 20 February 2012 / Accepted: 13 May 2012 / Published online: 26 May 2012

Abstract We report on an amperometric biosensor for hydrogen peroxide. It is obtained via layer-by-layer assembly of ordered mesoporous carbon nanospheres and poly(diallyldimethylammonium) on the surface of an indium tin oxide (ITO) glass electrode and subsequent adsorption of cytochrome *c*. UV–vis absorption spectroscopy was applied to characterize the process of forming the assembled layers. Cyclic voltammetry revealed a direct and quasi-reversible electron transfer between cytochrome *c* and the surface of the modified ITO electrode. The surface-controlled electron transfer has an apparent heterogeneous electron-transfer rate constant (k_s) of 5.9±0.2 s^{-1} in case of the 5-layer electrode. The biosensor displays good electrocatalytic response to the reduction of H_2O_2, and the amperometric signal increase steadily with the concentration of H_2O_2 in the range from 5 μM to 1.5 mM. The detection limit is 1 μM at pH 7.4. The apparent Michaelis-Menten constant (K_m) of the sensor is 0.53 mM. We assume that the observation of a direct electron transfer of cytochrome c on mesoporous carbon nanospheres may form the basis for a feasible approach for durable and reliable detection of H_2O_2.

Keywords Mesoporous carbon nanospheres · Layer-by-layer · Cytochrome c · Hydrogen peroxide · Biosensor

Electronic supplementary material The online version of this article (doi:10.1007/s00604-012-0834-1) contains supplementary material, which is available to authorized users.

Y. Wang · X. Bian · L. Liao · J. Zhu · K. Guo · J. Kong · B. Liu (✉)
Department of Chemistry, State Key Lab of Molecular Engineering of Polymers and Institute of Biomedical Sciences, Fudan University,
Shanghai 200433, People's Republic of China
e-mail: bhliu@fudan.edu.cn

Introduction

Hydrogen peroxide (H_2O_2) is not only an important intermediate species in food, pharmaceutical and environmental analysis, but also considered as the mediators of the cellular pathology in association with aging and severe human diseases such as cancers and cardiovascular disorders [1]. As a consequence, a sensitive method for reliable determination of H_2O_2 is necessary. Up to now, several traditional techniques were employed for H_2O_2 analysis, such as titrimetry, UV-visible spectrophotometry, fluorimetry, chemiluminescence, high performance liquid chromatography and electrochemistry. Among these methods, electrochemical biosensors display better prospect due to their advantages of easy preparation, fast detection, good selectivity, and low-cost [2]. Most previous studies on this subject involved the use of enzymes which can accelerate the electron transfer between the electrodes and H_2O_2 [3]. The heme protein cytochrome *c* (Cyt *c*) is an excellent model for studying the electron transfer of typical enzymes and is widely used to develop biosensors for the determination of H_2O_2 due to its close similarity to peroxidase [4]. However, the electron transfer at bare electrode surface is interrupted by the three-dimensional structure of enzymes because the redox active centers can be shielded by their insulated protein shells and unfavorable orientation on the electrode surface [5]. Moreover, direct adsorption of enzymes onto the electrode surface may frequently result in their denaturation and the loss of bioactivity. Therefore, a wealth of nanomaterials such as nanoparticles [6], nanotubes [7], nanoporous materials [8] are employed to immobilize the enzymes and at the same time, to connect the active center of redox enzymes to the electrode surface without the protein denaturing.

With the development of nanomaterials, nanoparticles with ordered mesostructures have been studied and have

attracted much attention in the fields of both nanotechnology and biomedicine in view of their property of the mesochannels and quantum effects in the nanoscale [9]. Their open-framework structures, large specific surface area, porosity, and nanosize make ordered mesoporous nanoparticles useful in catalysis [10], adsorption [11], controlled drugs release [12], and cellular delivery [13]. Benefiting from the advantages of carbon materials, such as good electrical conductivity, chemical inertness, and nontoxicity, carbon-based mesoporous nanoparticles are ideal carriage for metals, drugs and enzymes, paving a promising platform in biochemistry research [14]. Fang and coworkers demonstrated a novel low-concentration hydrothermal route to synthesize highly ordered mesoporous carbon nanoparticles with spherical morphology and uniform size [15]. The obtained mesoporous carbon nanospheres (MCNs) showed good biocompatibility and high drug capacity.

The layer-by-layer films assembled by alternative adsorption of positively and oppositely charged species from their solutions through electrostatic interactions have been reported as a robust method for facilitating electron transfer [16]. Moreover, layer-by-layer films can provide suitable microenvironments to retain the activity of biomolecules due to their mild conditions [17]. It has been wildly used in the investigation of direct electron transfer between proteins and underlying electrodes. For example, Shi and coworkers studied electrochemistry and electrocatalytic properties of hemoglobin in layer-by-layer films of SiO_2 with vapor-surface sol–gel deposition [18]. Xu et al. constructed a layer-by-layer assembled $(Hb/CMK\text{-}3)_n$ film for the fabrication of an amperometric H_2O_2 biosensor with high sensitivity and long-term stability [19].

Herein we described a new biosensor toward H_2O_2 using MCNs as the matrix for the immobilization of Cyt *c*. The MCNs were synthesized according to the previous report [15] and immobilized on the conducting indium/tin oxide (ITO) electrode via layer-by-layer assembly strategy. The Cyt *c* was absorbed onto multilayer of MCNs and the direct electrochemistry of Cyt *c* was investigated. The immobilized Cyt *c* showed a good electrocatalytic activity to the reduction of H_2O_2.

Experimental

Reagents and solutions

Horse heart cytochrome c (MW 12384), poly (diallyldimethylammonium chloride) (PDDA, an aqueous solution with a molecular weight of 100,000 – 200,000), and triblock copolymer Pluronic F127 (*Mw*=12600, $PEO_{106}PPO_{70}PEO_{106}$) were purchased from Sigma-Aldrich (http://www.sigmaaldrich.com). H_2O_2 (wt. 30 %), phenol, formalin aqueous solution (37 wt. %), and neat ethanol were purchased from Shanghai Chemical Plant (http://www.chinanusa.com). Stock solutions of H_2O_2 were freshly diluted from 30 % solution. The phosphate buffer solutions (PBS), in accordance with the physiological pH value of 7.4, were made of sodium phosphate (Na_2HPO_4: NaH_2PO_4=81:19, molar ratio) and NaCl dissolved in water at a final concentration of 50 and 10 mM, respectively. All other reagents were of analytical grade, and double distilled water was used throughout. ITO-coated glass plates with a square resistance of ~10 Ω cm^{-2} were purchased from Shenzhen Nanbo Display Technology Co. Ltd (http://www.csgholding.com/en/index.asp).

Synthesis of mesoporous carbon nanospheres

According to the previous report, ordered MCNs were prepared through an aqueous synthesis route containing low concentration reactants and promoted at a high temperature hydrothermal condition [15]. Briefly, commercial available triblock copolymer Pluronic F127 was employed as a template and phenolic resol as a carbon source. Firstly, 0.5 g of phenol, 1.75 mL of formalin aqueous solution (37 wt. %) and 15 mL of NaOH aqueous solution (0.1 M) were mixed and stirred at 70 °C for 0.5 h to obtain low-molecular-weight phernolic resols. Then 0.8 g of F127 dissolved in 15 mL of H_2O was added. The mixture was stirred at 66 °C with a stirring speed of 340±40 rpm for 2 h. After that, 50 mL water was added to dilute the solution. The reaction was stopped when the deposit was observed after 16~18 h. Until the deposit was dissolved again, 17.7 mL of the obtained solution was transferred into an autoclave and diluted with 56 mL of H_2O, then followed by heating at 130 °C for 24 h. The final MCNs products were obtained by carbonization at 700 °C in N_2 atmosphere for 3 h and the triblcok copolymer templates were removed during this process.

Preparation of the modified electrode

ITO-coated glass plates were thoroughly cleaned by sonicating sequentially for about 15 min in the following solvents: soapy water, neat ethanol, 1 M NaOH, distilled water and dried at room temperature. Then the prepared ITO electrode with original negative surface charge was treated with a polyelectrolyte of cationic PDDA (5 wt. %) for about 60 min to form positive surface charge. Afterwards, the electrode was alternately incubated in negatively charged suspension of MCNs (0.5 mg mL^{-1}) and PDDA for 20 min each. All of the adsorption steps were performed at ambient temperature and after each adsorption step the electrode was rinsed with distilled water. When this cycle procedure was repeated *N* times, the $(MCNs/PDDA)_N$/ITO electrode was obtained. Cyt *c* immobilization was achieved by immersing this modified electrode in Cyt *c* solution (0.5 mg mL^{-1},

dissolved in pH 7.4, 50 mM PBS) at 4 °C refrigerator overnight. Prior to all measurements, the modified electrode was rinsed in 50 mM pH 7.4 PBS to remove non-immobilized protein. Thus, the Cyt *c* modified electrode was obtained and will be referred as Cyt *c*/(MCNs/PDDA)$_N$/ITO electrode.

Apparatus

Scanning electron microscopy (SEM) images were recorded on a Philips XL30 microscope operated at 20 kV. Transmission electron microscopy (TEM) images were taken with a JEOL 2011 microscope operated at 200 kV. Cyclic voltammetric (CV) and amperometric measurements were carried out by a computer-controlled CHI 660c electrochemical workstation (CHI Instruments, Shanghai Chenhua Instrument Corp.). A three-electrode system was set up with the modified ITO as the working electrode, a coiled platinum wire as the counter electrode, and a saturated calomel electrode (SCE) as the reference in an electrochemical glass cell containing 10 mL 50 mM PBS at room temperature. A magnetic stirrer provided the convective transport during the amperometric measurement.

Results and discussion

Characterization of MCNs and Cyt *c*/(MCNs/PDDA)$_N$ assembled films

The morphology of MCNs was characterized by SEM and TEM. As shown in Fig. 1a, the typical SEM image displayed uniform spherical morphology of MCNs in large domains. The TEM image of synthesized MCNs showed uniform spheres with diameters of approximately 50 nm (Fig. 1b). Furthermore, it is remarkable that an ordered array of mesopores can be observed, implying an open pore structure on the surface. These characteristic nanospheres with mesostructures could be useful in adsorption, cellular delivery, and immobilization of biomolecules.

The position of the Soret band of iron heme is usually employed as an indicator of the microenvironment of heme proteins [20]. Figure 2 depicted the UV–vis absorption spectra of 0.5 mg mL^{-1} Cyt *c* in solution and the growth process of Cyt *c*/(MCNs/PDDA)$_N$ (N=1, 3, 5, 7) assembled films. As can be seen, the band for Cyt *c* adsorbed on the assembly is located at 408 nm, similar as that of native Cyt *c* in solution (409 nm). This implies that the MCNs matrix has good biocompatibility and is suitable for Cyt *c* molecules to maintain their native conformation and bioactivity. Moreover, with the increase of (MCNs/PDDA) bilayers, the absorption peak at 409 nm grew gradually, indicating an increase amount of Cyt *c* immobilized on (MCNs/PDDA)$_N$ assembled films.

Cyclic voltammetric behavior of Cyt *c* immobilized on (MCNs/PDDA)$_N$ assembled films

Cyclic voltammetry was employed to characterize the electron transfer behavior of Cyt *c* during the growth of the (MCNs/PDDA)$_N$ films. Typical voltammograms were shown in Fig. 3. A pair of well-defined and quasi-reversible redox peaks was observed in each of the cyclic voltammograms at ITO electrodes modified with Cyt *c*/(MCNs/PDDA)$_N$ (N=1, 3, 5, 7), while only the charge current was obtained at the (MCNs/PDDA)$_5$/ITO surface in 50 mM PBS (pH 7.4). The redox peaks can be attributed to the direct electron transfer of Cyt *c* on (MCNs/PDDA)$_N$ multilayer films. Moreover, both reduction and oxidation peaks grew gradually with the number of bilayers (N) up to 5, and then no longer increased with N. At the scan rate of 0.05 V s^{-1}, the formal potential ($E^0=(E_{pa}+E_{pc})/2$) of Cyt *c*

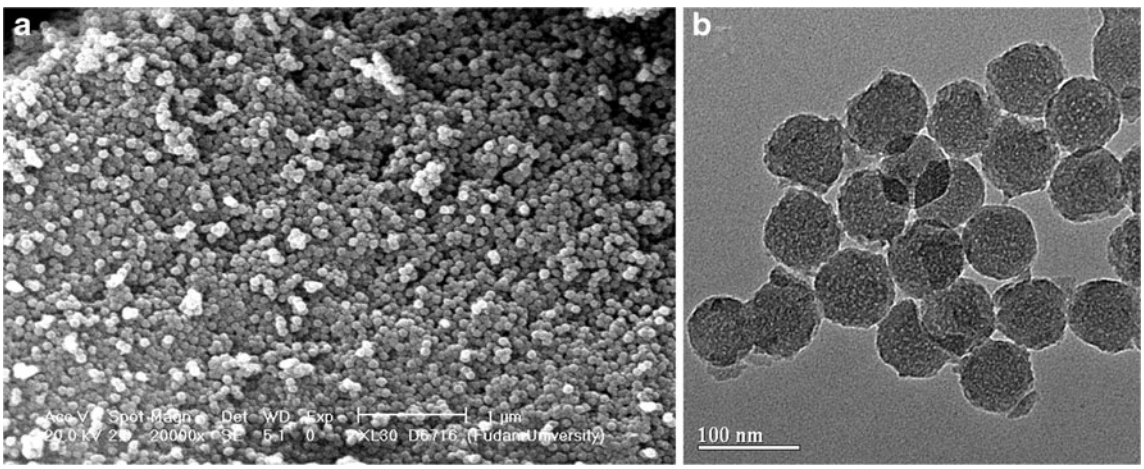

Fig. 1 (**a**) SEM image of MCNs. (**b**) TEM image of MCNs

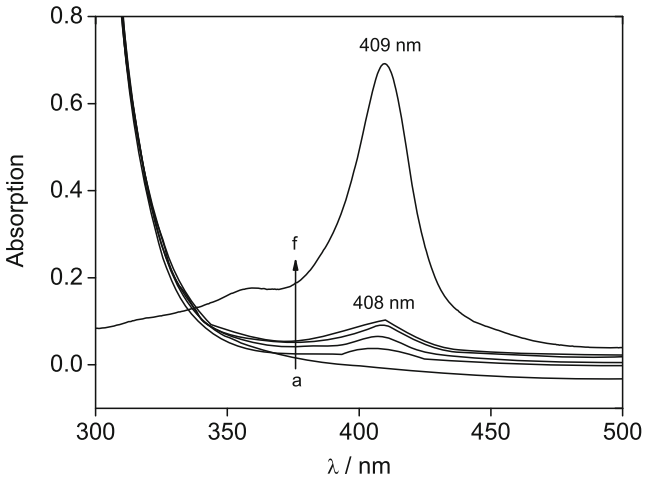

Fig. 2 UV–vis absorption spectra of bare ITO electrode (curve a), Cyt *c*/(MCNs/PDDA)$_N$/ITO (*N*=1, 3, 5, 7, curve b, c, d, e, respectively), and 0.5 mg mL^{-1} Cyt *c* in 50 mM PBS (pH 7.4, curve f)

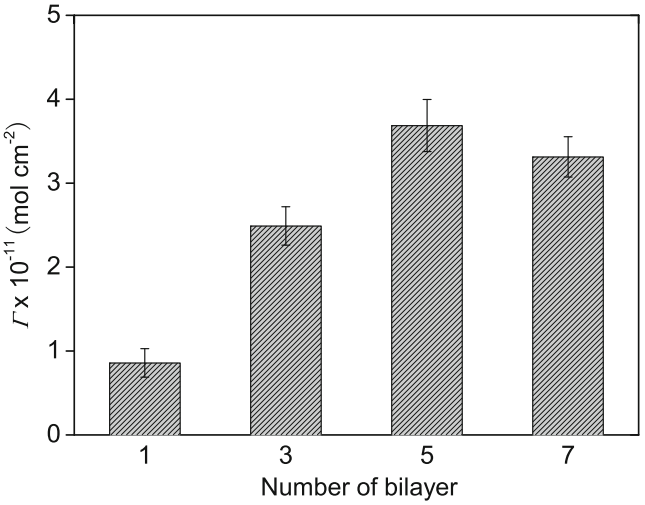

Fig. 4 Surface coverage of electrochemical addressable Cyt *c* immobilized in different number of bilayers of (MCNs/PDDA)$_N$ (*N*=1, 3, 5, 7)

obtained at the (MCNs/PDDA)$_5$/ITO electrode is estimated to be 0.141 V (vs. SCE) and a peak-to-peak potential separation (ΔE_p) of the redox peaks is about 0.032 V. Compared with the E^0 of Cyt *c* in solution with its native state [21], the E^0 of Cyt *c* at MCNs matrix shifted positively. Previous studies have demonstrated that E^0 is sensitive to the protein conformation and the solvent medium [22]. A small change in the accessibility of the heme group to the protein exterior can modulate the heme reduction potential dramatically. In the present study, the electrostatic interaction between the positively charged Cyt *c* (pI=10.5) and negatively charged carbon surface led to a slight conformation change, which accounted for the shift of E^0 in our experiment. The small ΔE_p indicated a fast electron transfer rate between Cyt *c* and (MCNs/PDDA)$_N$/ITO electrode.

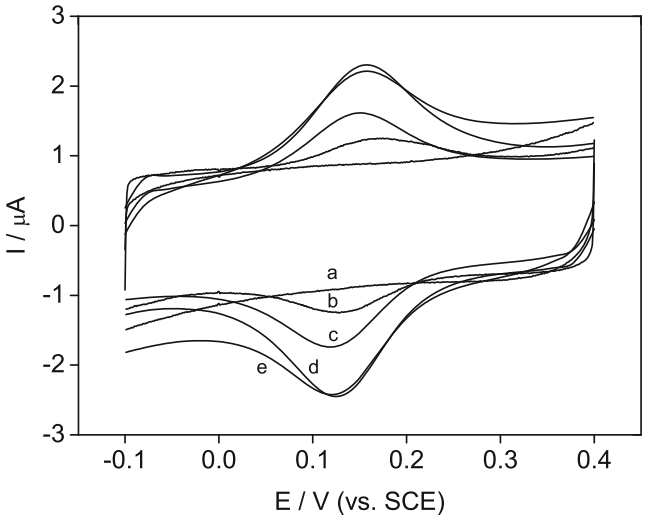

Fig. 3 Cyclic voltammograms of the bare ITO electrode (curve a), and Cyt *c*/(MCNs/PDDA)$_N$/ITO (*N*=1, 3, 5, 7, curve b, c, d, e, respectively) electrodes in 50 mM PBS (pH 7.4). Scan rate: 0.05 V s^{-1}

Former research proved that the negative charged surface can promote the attachment of Cyt *c* in an orientation favorable for electron transfer [23]. Thus, the mesoporous carbon nanospheres can provide a favorable microenvironment for the direct electron transfer of Cyt *c*.

The average surface concentration (Γ, mol cm^{-2}) of electroactive Cyt *c* molecules can be estimated from the charge integration of the reduction peak of the cyclic voltammogram of Cyt *c*/(MCNs/PDDA)$_N$/ITO, according to the Faraday's law. As shown in Fig. 4, the Γ of Cyt *c* increased gradually with the number of bilayers (*N*) up to 5, and then decreased slightly. We speculate that with the increase of *N*, the distance from proteins in outer layers to the electrode surface was extended accordingly. Cyt *c* molecules in those layers are not electrochemically addressable at fast scan rates [18]. Thus, a good communication between Cyt *c*

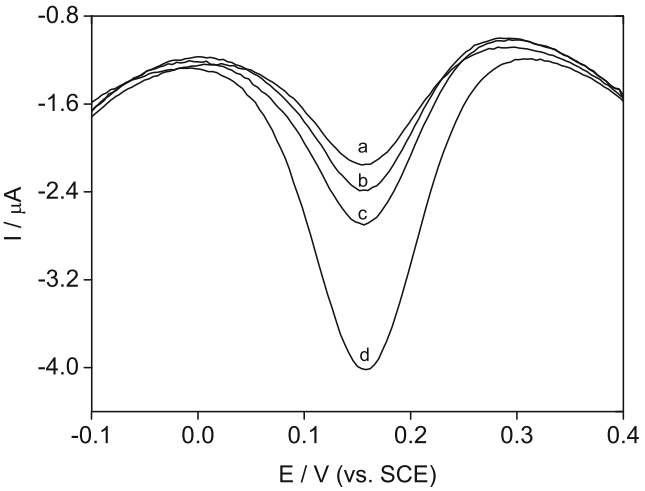

Fig. 5 Differential pulse voltammograms obtained at Cyt *c*/(MCNs/PDDA)$_5$/ITO electrode in 50 mM PBS (pH 7.4) containing (a) 0 μM, (b) 50 μM, (c) 100 μM, (d) 300 μM H_2O_2

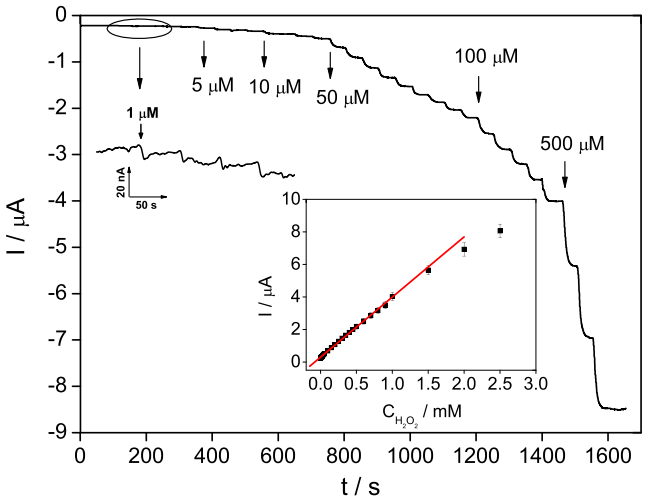

Fig. 6 Typical amperometric response of Cyt *c*/(MCNs/PDDA)$_5$/ITO electrode to successive addition of H_2O_2 into 10 mL PBS (50 mM, pH 7.4) at the applied potential of −0.25 V. Inset is the calibration curve of the responses of Cyt *c*/(MCNs/PDDA)$_5$/ITO electrode to H_2O_2

molecules and the electrode surface was maintained when the number of bilayer is as high as 5. In this work, Cyt *c* molecules immobilized on five layers of (MCNs/PDDA), designated as Cyt *c*/(MCNs/PDDA)$_5$/ITO, were chosen in the following experiments.

To further investigate the characteristics of Cyt *c* immobilized on the multilayer films, the effect of scan rates on the voltammetric behavior of Cyt *c* was studied. In the range from 0.02 to 0.1 V s^{-1}, both the anodic and cathodic peak currents vary linearly with the potential scan rate, indicating a surface-controlled electrochemical process (Electronic Supplementary Material, Fig. S1). According to Laviron theory [24], the charge transfer coefficient (α) was calculated as 0.49. And the heterogeneous electron transfer rate constant (k_s) between the electrode and the surface modification layer was estimated to be 5.9±0.2 s^{-1}. The k_s value is comparable to the value for Cyt *c* immobilized on the WO_3 nanoparticles film modified electrode (5.57± 0.54 s^{-1}) [25], and higher than those of Cyt *c* immobilized on nanozeolite-assembled electrode (2.2 s^{-1}) [26], mesoporous materials (2.2 s^{-1}) [27], and multi-walled carbon nanotubes (4.0±0.2 s^{-1}) [28]. The fast electron transfer rate indicates that the host matrix of MCNs offers an ideal microenvironment for facilitating electron transfer between Cyt *c* and the electrode.

Amperometric response toward H_2O_2 based on Cyt *c*/(MCNs/PDDA)$_5$/ITO

Figure 5 showed differential pulse voltammogram of Cyt *c*/(MCNs/PDDA)$_5$/ITO electrode in the absence and presence of H_2O_2 in 50 mM PBS (pH 7.4). The current responses increased with the H_2O_2 concentration, indicating the electrocatalytic activity of the immobilized Cyt *c* for the reduction of H_2O_2. The typical amperometric responses of the enzyme electrode to successive concentration changes of H_2O_2 were examined at pH 7.4 and the applied potential of −0.25 V. The corresponding current-time responses are shown in Fig. 6. Well-defined steady state current responses were obtained at Cyt *c*/(MCNs/PDDA)$_5$/ITO electrode, and the currents increased stepwisely with successive additions of H_2O_2. The response time $t_{90\%}$ (reaching 90 % of the maximum response) was less than 6 s, which indicated a fast process and the immobilized Cyt *c* could well catalyze the reduction of H_2O_2. The inset of Fig. 6 corresponds to the calibration plot of the prepared biosensor. The currents had a linear relationship with the concentration of H_2O_2 in the range of 5 μM to 1.5 mM with a correlation coefficient of 0.9991 (n=22) and the detection limit was examined

Table 1 Comparison of the performance of H_2O_2 biosensors based on layer-by-layer assembly strategy

Methods	Applied potential (V)	Linear range (μM)	Detection limit (μM)	Reference
Cyt c/(MCNs/PDDA)$_5$/ITO	−0.25	5–1.5×10^3	1.0	This work
Cyt c/(nano-LTL-zeolite/PDDA)$_5$/ITO	−0.25	15–540	0.0032	[26]
(Hb/SiO_2)$_6$/PDDA/GCE	−0.30	1–200	0.5	[18]
(Hb/CMK-3)$_6$	–	1.2–57	0.6	[19]
Hemin/(PEI-CMC)$_5$PEI/GCE	−0.60	5–1.0×10^3	5	[31]
(Zeolite/Hb)$_7$/pyrolytic graphite disk	0	50–1.0×10^3	5	[32]
(MB-MWNTs/HRP)$_5$/gold electrode	−0.20	4.0–3.78×10^3	1.0	[33]
HRP/(PA/GNPs)$_2$/gold electrode	−0.10	6.5–14	3.3	[34]
HRP/$AuNP_4$/GCE	−0.40	9.8–6.0×10^3	4.9	[35]

MCN mesoporous carbon nanospheres; *Nano-LTL-zeolite* nanometer-sized Linder type-L zeolite; *Hb* Hemoglobin; *CMK-3* mesoporous carbon; *PEI-CMC* poly(ethyleneimine) and carboxymethyl cellulose hybrid film; *HRP* horseradish peroxidase; *MB-MWNTs* methylene Blue-multiwalled carbon nanotubes; *PA* phytic acid; *GNPs* gold nanoparticles; *$AuNP_4$* four-layer Au nanoparticles films

to be 1 μM. The analytical performances of the biosensor were summarized in Table 1 and compared with other layer-by-layer assembly-based biosensors towards H_2O_2 in terms of detection limit and linear response range. It can be seen that Cyt *c*/(MCNs/PDDA)$_5$/ITO offers a reasonable linear range for H_2O_2 detection with a lower detection limit.

The apparent Michaelis-Menten constant (K_m) provides an indication of both the enzymatic affinity to the substrate and the ratio of microscopic kinetic constants. It can be calculated from the Lineweaver-Burk equation [29]:

$$1/I_{ss} = 1/I_{\max} + K_m/I_{\max}C$$

Where I_{ss} is the steady-state current after the addition of substrate, which can be obtained from amperometric experiments, I_{max} is the maximum current under saturated substrate condition and C is the bulk concentrate of the substrate. The value of K_m can be calculated from the slope (K_m/I_{max}) and the intercept ($1/I_{max}$) for the plot of the reciprocals of the steady-state current (I_{ss}) vs. H_2O_2 concentration (C). The K_m value for the Cyt *c*/(MCNs/PDDA)$_5$/ITO electrode is estimated to be 0.53 mM, indicating that the Cyt *c* immobilized on the (MCNs/PDDA)$_5$ assembled electrode retains its bioactivity.

In addition, at the applied potential of −0.25 V, the influence of possible interfering species on the current response of the sensor was examined (Electronic Supplementary Material, Fig. S2). The present biosensor was free from the interferences like uric acid (UA), glucose, NO_2^-, NO_3^-, and SO_3^{2-} (<2 %). A slight interference (8.5 %) of response currents to 100 μM ascorbic acid (AA) was observed relative to 100 μM H_2O_2. This interference could be further reduced by using Nafion membranes on the electrode surfaces [30].

Reproducibility and stability of the Cyt *c*/(MCNs/PDDA)$_5$/ITO electrode

The repeatability of biosensor was evaluated in the current response for successive addition of 100 μM H_2O_2 at −0.25 V with the same enzyme electrode. The relative standard deviation (R.S.D.) was 4.8 % for nine successive assays. The electrode-to-electrode reproducibility was determined with the same addition of H_2O_2 using 3 different enzyme electrodes. It shows an acceptable reproducibility with a R.S.D. of 3.1 %. The stability of the biosensor was also examined. No obvious change in cyclic voltammogram was observed when 100 continuous cyclic scans were repeated in 50 mM PBS (pH 7.4) with a scan rate of 0.05 V s^{-1}. When not in use, the electrode was stored in the refrigerator at 4 °C. After 7 days, the amperometric responses of the modified electrode retained 90 % of its initial value, and after 20 days the responses remained 82 %.

Conclusions

A uniform and stable multilayer membrane of (MCNs/PDDA)$_N$ were constructed via a simple layer-by-layer assembly strategy and used as enzyme immobilization matrix to fabricate Cyt *c*/(MCNs/PDDA)$_N$/ITO electrodes. The direct electrochemistry of Cyt *c* was achieved on the multilayer films modified electrode. Moreover, the resulted Cyt *c*/(MCNs/PDDA)$_5$/ITO electrode showed a good electrochemical activity to the reduction of H_2O_2. The presented biosensor exhibited fast amperometric response, wide linear range, low detection limit and good reproducibility.

Acknowledgments This work was supported by NSFC (20925517, 21175028) and SKLEAC201101. Y. Wang and X. Bian contributed equally to this work.

References

1. Hall ED, Braughler JM (1989) Central nervous-system trauma and stroke II. Physiological and pharmacological evidence for involvement of oxygen radicals and lipid-peroxidation. Free Radical Bio Med 6:303–313
2. Park BW, Yoon DY, Kim DS (2010) Recent progress in biosensing techniques with encapsulated enzymes. Biosens Bioelectron 26:1–10
3. Song J, Xu JM, Zhao PS, Lu LD, Bao JC (2011) A hydrogen peroxide biosensor based on direct electron transfer from hemoglobin to an electrode modified with Nafion and activated nanocarbon. Microchim Acta 172:117–123
4. Yagati AK, Lee T, Min J, Choi JW (2012) Electrochemical performance of gold nanoparticle–cytochrome c hybrid interface for H_2O_2 detection. Colloids Surf B Biointerfaces 92:161–167
5. Xu Q, Mao C, Liu NN, Zhu JJ, Sheng J (2006) Direct electrochemistry of horseradish peroxidase based on biocompatible carboxymethyl chitosan-gold nanoparticle nanocomposite. Biosens Bioelectron 22:768–773
6. Huang JM, Zheng JB, Sheng QL (2011) Direct electrochemistry of myoglobin based on electrodeposition of Pd nanoparticles with carbon ionic liquid electrode as basic electrode. Microchim Acta 173:157–163
7. Xu SX, Zhang XF, Wan T, Zhang CX (2011) A third-generation hydrogen peroxide biosensor based on horseradish peroxidase cross-linked to multi-wall carbon nanotubes. Microchim Acta 172:199–205
8. Wang Y, Qian K, Guo K, Kong JL, Marty JL, Yu CZ et al (2011) Electrochemistry and biosensing activity of cytochrome c immobilized in macroporous materials. Microchim Acta 175:87–95
9. Lu F, Wu SH, Hung Y, Mou CY (2009) Size effect on cell uptake in well-suspended, uniform mesoporous silica nanoparticles. Small 5:1408–1413
10. Li C (2004) Chiral synthesis on catalysts immobilized in microporous and mesoporous materials. Catal Rev 46:419–492
11. Lu ZD, Ye MM, Li N, Zhong WW, Yin YD (2010) Self-assembled TiO_2 nanocrystal clusters for selective enrichment of intact phosphorylated proteins. Angew Chem Int Ed 49:1862–1866
12. Slowing II, Vivero-Escoto JL, Wu CW, Lin VSY (2008) Mesoporous silica nanoparticles as controlled release drug delivery and gene transfection carriers. Adv Drug Deliver Rev 60:1278–1288

13. Kim TW, Chung PW, Slowing II, Tsunoda M, Yeung ES, Lin VSY (2008) Structurally ordered mesoporous carbon nanoparticles as transmembrane delivery vehicle in human cancer cells. Nano Lett 8:3724–3727
14. Yan AH, Lau BW, Weissman BS, Kulaots I, Yang NYC, Kane AB et al (2006) Biocompatible, hydrophilic, supramolecular carbon nanoparticles for cell delivery. Adv Mater 18:2373–2378
15. Fang Y, Gu D, Zou Y, Wu ZX, Li FY, Che RC et al (2010) A low-concentration hydrothermal synthesis of biocompatible ordered mesoporous carbon nanospheres with tunable and uniform size. Angew Chem Int Ed 49:7987–7991
16. Zheng LZ, Yao X, Li JH (2006) Layer-by-layer assembly films and their applications in electroanalytical chemistry. Curr Anal Chem 2:279–296
17. Tedeschi C, Li LD, Mohwald H, Spitz C, von Seggern D, Menzel R et al (2004) Engineering of layer-by-layer coated capsules with the prospect of materials for efficient and directed electron transfer. J Am Chem Soc 126:3218–3227
18. Shi GY, Sun ZY, Liu MC, Zhang L, Liu Y, Qu YH et al (2007) Electrochemistry and electrocatalytic properties of hemoglobin in layer-by-layer films of SiO_2 with vapor-surface sol–gel deposition. Anal Chem 79:3581–3588
19. Feng JJ, Xu JJ, Chen HY (2007) Direct electron transfer and electrocatalysis of hemoglobin adsorbed on mesoporous carbon through layer-by-layer assembly. Biosens Bioelectron 22:1618–1624
20. George P, Hanania G (1953) A spectrophotometric study of ionizations in methaemoglobin. Biochem J 55:236–243
21. Hawkridg FM, Kuwana T (1973) Indirect coulometric titration of biological electron-transport components. Anal Chem 45:1021–1027
22. Wang SF, Chen T, Zhang ZL, Shen XC, Lu ZX, Pang DW et al (2005) Direct electrochemistry and electrocatalysis of heme proteins entrapped in agarose hydrogel films in room-temperature ionic liquids. Langmuir 21:9260–9266
23. Kuznetsov BA, Byzova NA, Shumakovich GP (1994) The effect of the orientation of cytochrome-c molecules covalently attached to the electrode surface upon their electrochemical activity. J Electroanal Chem 371:85–92
24. Laviron E (1979) General expression of the linear potential sweep voltammogram in the case of diffusionless electrochemical systems. J Electroanal Chem 101:19–28
25. Deng ZF, Gong YC, Luo YP, Tian Y (2009) WO_3 nanostructures facilitate electron transfer of enzyme: application to detection of H_2O_2 with high selectivity. Biosens Bioelectron 24:2465–2469
26. Yu T, Zhang YH, You CP, Zhuang JH, Wang B, Liu BH et al (2006) Controlled nanozeolite-assembled electrode: remarkable enzyme-immobilization ability and high sensitivity as biosensor. Chem-Eur J 12:1137–1143
27. Zhu L, Wang KQ, Lu TH, Xing W, Li J, Yang XG (2008) The direct electrochemistry behavior of Cyt c on the modified glassy carbon electrode by SBA-15 with a high-redox potential. J Mol Catal B: Enzym 55:93–98
28. Zhao GC, Yin ZZ, Zhang L, Wei XW (2005) Direct electrochemistry of cytochrome c on a multi-walled carbon nanotubes modified electrode and its electrocatalytic activity for the reduction of H_2O_2. Electrochem Commun 7:256–260
29. Kamin RA, Wilson GS (1980) Rotating-ring-disk enzyme electrode for biocatalysis kinetic-studies and characterization of the immobilized enzyme layer. Anal Chem 52:1198–1205
30. Wu KB, Hu SS (2004) Electrochemical study and selective determination of dopamine at a multi-wall carbon nanotube-Nafion film coated glassy carbon electrode. Microchim Acta 144:131–137
31. Wang BZ, Du XY, Wang MQ, Gong WL, Anzai J (2008) A facile preparation of H_2O_2 sensors using layer-by-layer deposited thin films composed of poly(ethyleneimine) and carboxymethyl cellulose as matrices for immobilizing hemin. Electroanal 20:1028–1031
32. Xie Y, Liu HY, Hu NF (2007) Layer-by-layer films of hemoglobin or myoglobin assembled with zeolite particles: Electrochemistry and electrocatalysis. Bioelectrochemistry 70:311–319
33. Zhang YM, Liu LJ, Xi FN, Wu TX, Lin XF (2010) A simple layer-by-layer assembly strategy for a reagentless biosensor based on a nanocomposite of methylene blue-multiwalled carbon nanotubes. Electroanal 22:277–285
34. Wang Y, Ma XL, Wen Y, Zheng YQ, Duan GP, Zhang ZR et al (2010) Phytic acid-based layer-by-layer assembly for fabrication of mesoporous gold film and its biosensor application. J Electrochem Soc 157:K5–K9
35. Li WT, Wang MH, Li YJ, Sun Y, Li JC (2011) Linker-free layer-by-layer self-assembly of gold nanoparticle multilayer films for direct electron transfer of horseradish peroxidase and H_2O_2 detection. Electrochim Acta 56:6919–6924